Composites: Part A 177 (2024) 107943

Contents lists available at ScienceDirect

Composites Part A

journal homepage: www.elsevier.com/locate/compositesa

Harnessing the power of carbon fiber reinforced liquid crystal elastomer composites for high-performance aerospace materials: A comprehensive investigation on reversible transformation and shape memory deformation

Yuliang Xia [a], Tong Mu [a], Yanju Liu [b,*], Jinsong Leng [a,*]

[a] Centre for Composite Materials and Structures, Harbin Institute of Technology (HIT), No. 2 Yikuang Street, P.O. Box 3011, Harbin 150080, People's Republic of China
[b] Department of Astronautical Science and Mechanics, Harbin Institute of Technology (HIT), P.O. Box 301, No. 92 West Dazhi Street, Harbin 150001, People's Republic of China

ARTICLE INFO

Keywords:
A. Polymer-matrix composites (PMCs)
A. Smart materials
Liquid crystalline elastomer composites

ABSTRACT

Liquid Crystal Elastomers (LCEs) showcase transformative features making them suitable for rigorous applications, notably aerospace. However, their standalone mechanical properties often fall short. This study introduces the incorporation of carbon fiber to form a reinforced LCE composite, LCEC, aimed at enhancing mechanical performance while maintaining reversible deformation and shape memory attributes. Molecular-level analysis indicates an upsurge in overall composite performance with improved storage modulus (1.1 GPa at 25 °C), heightened reversible deformation, and better shape memory functionality. Both materials retain transformation properties under gamma-ray irradiation. This investigation into LCE and LCEC performance underscores their potential in demanding environments due to improved mechanical strength, transformability, shape memory performance, and radiation resistance. The research offers insights into micro-level alterations leading to macro-level enhancements in material properties, paving the way for future advancements in fields like robotics and aerospace.

1. Introduction

Materials that exhibit the ability to adapt their unique characteristics in response to external stimuli, known as smart materials, have garnered significant interest. Their potential to revolutionize sectors such as aerospace, robotics, and biomedical engineering due to their tunable characteristics underscores their importance in contemporary research. [1–8]. LCEs as a particularly promising category among smart materials display reversible deformation and shape memory behavior[9–16]. These materials are characterized by their mesogenic moieties, which impart anisotropic mechanical properties and enable reversible transformations[17]. LCEs have shown potential in applications that require dynamic and adaptive systems, such as actuators, sensors, and artificial muscles[18–22]. Nevertheless, to fully harness their potential in such applications, enhancing their mechanical performance is a necessity - a challenge that continues to be a prominent hurdle in this field.

Despite these remarkable properties of LCEs, one of the current challenges lies in enhancing their mechanical performance to fulfill the demanding requirements of different applications. Composite materials, such as those incorporating nano particles, have been considered as a potential solution[23–27]. Previous scholarly endeavors have primarily concentrated on the synthesis and characterization of LCEC, aiming to achieve desirable transformable structures and enhanced transformation attributes. [28–32]. Nevertheless, these methodologies seem to offer limited advancements in augmenting the mechanical properties of the materials. The dispersed particles, under these conventional methods, appear to contribute minimally to the enhancement of the matrix's mechanical attributes.

Contrary to dispersed particles, continuous fibers of considerable length serve a more substantial part in enhancing the mechanical properties of polymer composites. Carbon fibers, renowned for their remarkable tensile strength and lightweight characteristics, have been widely applied in composite materials spanning different applications, including those within the aerospace and automotive industries[33–35]. The incorporation of carbon fibers within LCE matrices might potentially induce synergistic effects that bolster mechanical performance whilst sustaining or augmenting their smart properties. Nevertheless, unresolved challenges and areas demanding improvement persist, such

* Corresponding authors.
E-mail addresses: yj_liu@hit.edu.cn (Y. Liu), lengjs@hit.edu.cn (J. Leng).

https://doi.org/10.1016/j.compositesa.2023.107943
Received 31 August 2023; Received in revised form 24 October 2023; Accepted 29 November 2023
Available online 1 December 2023
1359-835X/

as discerning the impacts of carbon fiber integration on mesogen orientation, understanding the function of interfacial bonding between the LCE matrix and carbon fibers, and examining the stability of LCEs and their composites under harsh environmental conditions, inclusive of gamma-ray irradiation exposure. The advancement of fabrication techniques and processing methodologies that optimize the integration of carbon fibers into LCE matrices is crucial for unlocking the full potential of these composite materials.

In this study, we aim to address these challenges by preparing LCE pure material and its carbon fiber reinforced composite, LCEC, and investigating their mechanical performance, reversible deformation, shape memory properties, and stability under gamma-ray irradiation. Through a comprehensive experimental approach, we seek to gain valuable insights into the behavior of these materials and identify innovative strategies for enhancing their performance. We examined the effects of carbon fiber incorporation on mesogen orientation, the role of interfacial bonding between the LCE matrix and carbon fibers, and the influence of gamma-ray irradiation on the materials' properties. Anticipated to pioneer the evolution of advanced smart materials, our research introduces fresh perspectives on the construction and development of LCE-based composites. By enhancing their mechanical performance, intelligent responsiveness, and stability in varying environments, we aim to elevate their potential for diverse applications.

2. Experiment method

The experiment was conducted to prepare the LCE pure material and its carbon fiber composite material. The gamma radiation resistance test, as well as the reversible deformation and unidirectional shape memory polymer (SMP) properties were performed. The details of the experiment method are as follows:

2.1. Materials

Directly applied without further treatment, the following materials were used: pentaerythritol tetra(3-mercaptopropionate) (PEMP, Sigma-Aldrich Corp.), 2-Methyl-1,4-phenylene bis(4-(3-(acryloyloxy)propoxy) benzoate) (RM 257, HCCH Company), 4-(2-Hydroxyethoxy)phenyl 2-hydroxy-2-propyl ketone (HHMP, UV initiator, Sigma-Aldrich Corp.), tetrahydrofuran (THF, Sigma-Aldrich Corp.), triethylamine (TEA, Sigma-Aldrich) (Fig. 1**a**), and unidirectional carbon fiber cloth (Toray T300B-1000-50B). In order to prepare a catalytic solution, TEA was diluted in THF solvent at a mass ratio of 1:50.

2.2. Preparation of LCE actuators

RM257 (8 g), PEMP (2.88 g), THF (2 g), and HHMP (0.22 g, 2 % wt%) have been combined in a 50 ml flask. The mixture was then heated under 80 °C in 1 min to form a transparent solution. Subsequently, catalytic solution (0.054 g, 0.5 wt%) have been transferred into the mixture and stirred for 1 min following by pouring into a Teflon mold featuring a cubic groove with 2 mm deep. In the fabrication of LCE composites, a layer of unidirectional carbon fiber cloth was placed on the mold's surface before pouring the solution. Polydomain LCE composites were acquired after vacuuming the solution for 2 min, curing it under 25 °C overnight. The polydomain LCE underwent a treatment at 80 °C under vacuum conditions for a duration of 24 h to facilitate the removal of the THF solvent. The cured sample has been then cut in a cuboid measuring 40 × 15 × 2 mm. Longitudinal axis of the composite material has been set perpendicular to the carbon fiber axis. Monodomain LCE actuators with a uniform orientation were prepared by bending the polydomain LCE samples at 180° and fixing them after 10 min of ultraviolet (UV) irradiation (50 mW cm^{-2}) (Fig. 1**b**). The angle, denoted as alpha (α), is formally defined as the angular separation between the tangent lines drawn at both extremities of the actuator.

The materials were subsequently classified into two groups: LCE and LCE composite. Vacuum gamma-ray irradiation tests were conducted. Samples were exposed to varying intensities of gamma radiation. The administered gamma-ray irradiation doses included 10 KGy and 1000 KGy. These unirradiated samples were designated as LCE and LCEC, while the irradiated samples were labeled as LCE10, LCE1000, LCEC10, and LCEC1000. The gamma irradiation procedure was executed using a cobalt-60 source, with the samples positioned at a consistent distance from the source to ensure a uniform radiation dose.

2.3. Characterization

Infrared spectroscopy (FTIR) was used to generate individual spectral data for each specimen under normal environmental conditions, employing spectral resolution of 2 cm^{-1} with 40 scans in total.

Two-dimensional wide-angle X-ray diffraction (2D-XRD) methodology was utilized to ascertain the anisotropic alignment of our specimens, focusing particularly on those with monodomain characteristics.

We utilized dynamic mechanical analysis (DMA) to gauge the mechanical attributes of the samples across a wide temperature spectrum, from −50 °C to 200 °C, employing heating rate of 5 °C min^{-1} and a 1 Hz frequency.

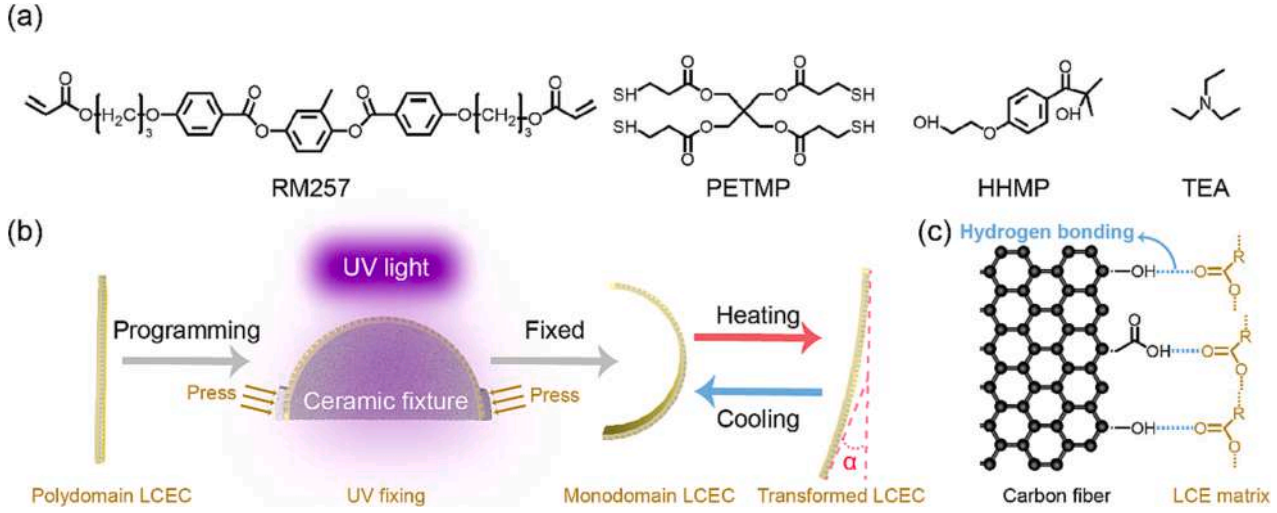

Fig. 1. Schematic of the fabrication process of LCEC actuators. (a) Chemical structure of monomers for preparing LCEC actuators; (b) Processes of fabricating LCEC actuators with different stretching angle between LCE matrix and carbon fiber; (c) Microscopic representation of hydrogen bonding interactions between the carbon fiber and the LCE matrix.

The mechanical properties for standard tensile specimens were evaluated before and after exposure to gamma-ray radiation using a universal testing machine with a 5 kN load cell. These tensile tests have been conducted with an elongation rate of 2 mm s^{-1} at ambient condition.

In a nitrogen atmosphere, the transition temperature of our samples has been evaluated by applying differential scanning calorimetry (DSC). These measurements involved cycling temperatures from −30 °C to 200 °C and vice versa with a rate of 5 °C/min.

We analyzed fiber content and thermal stability of the polymer and their composites using thermogravimetric analysis (TGA), where we subjected these samples in temperatures ranging from room temperature to 800 °C with a heating rate of 10 °C/min.

Microstructural assessment of the samples was achieved using scanning electron microscopy, which allowed us to observe their morphology at a high level of detail.

We conducted reversible actuation testing by thermally actuating the samples from room temperature to 120 °C in 90 s, followed by a cooling period of 300 s.

For the Shape memory property testing, samples were first heated to 120 °C, and upon reaching this temperature, the angle was flattened to 0° before cooling and shaping under external force. After 120 s of cooling, the sample was reheated using a heat gun. We evaluated the efficiency of the shape memory characteristics for these samples by calculating rates of shape fixity (R_f) and shape recovery (R_r) through following formulas:

$$R_f = \frac{180 - \alpha}{180 - \alpha_{load}} \times 100\%$$

$$R_r = \frac{180 - (\alpha - \alpha_{rec})}{180 - \alpha} \times 100\%$$

where α represents fixed angle after cooling to the room temperature with load removed, α_{load} is the angle when maximum load is applied, and α_{rec} indicates the angle after the recovery process.

3. Results and discussion

Our synthesis of LCE composite involved a one-click chemistry and a two-step cross-linking method, in combination with the integration of a unidirectional carbon fiber cloth. Firstly, monomers RM257 and thiol PEMP were combined in a stoichiometric ratio to form a pre-polymer. The thiol group reacted with the acrylic group in the presence of an appropriate catalyst, TEA, resulting in a thiol-ene click reaction. The reaction mechanism involves a radical addition process, where the thiol group adds to the carbon–carbon double bond of the acrylic group. This step leads to the forming of thioether linkage, connecting these monomers and forming loose network of the LCE material.

In the second step, a photoinitiator (HHMP) has been transferred into the pre-polymer mixture, which has been then heated at 80 °C for 1 min, resulting in a molten solution. The mixture was poured into the mold with a layer of carbon fiber cloth placed on the mold's surface. This step ensured to form a strong interface between the LCE matrix with the carbon fiber reinforcement. Polydomain LCE composites were acquired after vacuuming the sample for two minutes, cooling it to room temperature for 24 h, and completing the demolding process. The sample was then cut into a cuboid measuring 40 × 15 × 2 mm.

Lastly, samples have been exposed to UV light to generate free radicals from the photoinitiator. These radicals then initiated the cross-linking process between the remaining thiol and acrylic groups, lead the forming of a more robust network. Monodomain LCE actuators with a uniform orientation were prepared by bending the polydomain LCE samples at 180° and fixing them after 10 min of UV radiation. In the previous publications, it was established that the surface of Toray carbon fibers had undergone an oxidation and modification process, resulting in the presence of hydroxyl and carboxyl groups[36]. The synthesized polymer in our current work encompasses an abundance of ester groups. These ester constituents can form hydrogen bonds with the hydroxyl and carboxyl groups, thus enhancing the adherence between the LCE matrix and the carbon fibers (Fig. 1**c**).

3.1. Spectra analysis

In our study, we carried out spectroscopic evaluations to understand the progress of the chemical reaction during the formation of the polymer. We used a technique known as FTIR to recognize distinct groups of molecular within the polymer. It was observed in all the samples that the particular group linked to thiol, originally peaking at 2568 cm^{-1}, vanished, while the one linked to acrylate (peak at 810 cm^{-1}) remained present after the thiol-acrylate reaction. These findings provide evidence that thiol units and some acrylate units took part in the formation process, which aligns with our anticipated pathway for the creation of the polymer (Fig. 2). Notably, a broadening of the ester group peak position at 1724 cm^{-1} was identified in the LCEC as opposed to the LCE. This can be attributed to the hydrogen bonding interactions between the LCE and the carbon fiber, as depicted in **Figure S4**.

We assessed the liquid crystal order changes by conducting 2D-WAXD experiments on samples at room temperature (Fig. 3**a**). The Debye ring observations from the 2D-WAXD experiments effectively identified sample orientation at the microscopic level. Taking into account that the potential impact of unidirectional carbon fibers on the Debye rings obtained through 2D-XRD, we also conducted additional testing on the Debye rings acquired from LCEC samples that had not undergone bending and shaping. LCE, LCEC, and polydomain LCEC each display a peak with a certain width at $2\theta = 19.54°$, representing a d-space of 4.53 Å (Fig. 3**b**) . Furthermore, LCEC and polydomain LCEC exhibit a high-intensity peak at $2\theta = 2.86°$, representing a d-space of 30.85 Å, which is absent in LCE. Consequently, we postulate that this peak could be attributed to the presence of carbon fibers. LCEC also exhibits a subtle peak at $2\theta = 25.26°$, representing a d-space of 3.52 Å (Fig. 3**c and 3d**). This peak position is ascribed to the interactions between the LCE and the carbon fiber, emphasizing that the presence of hydrogen bonding significantly influences the microstructure of LCE. In the azimuth integration, the peak position of LCE is not obvious, while LCEC and polydomain LCEC have obvious peak positions (**Figure S1**).

The findings demonstrate that the Debye rings of pure materials display no discernible orientation, which markedly contrasts with the results documented in our previously published articles[34]. We surmise that the primary cause of this difference is the distinct preparation methods employed for the materials. In the earlier report, we utilized a pre-stretching technique on the sample, which facilitated improved mesogen orientation at the microscopic level. However, in the current experiment, the material's high modulus rendered it impractical to apply pre-stretching treatment to the sample. As a result, we adopted a bend-setting approach, which may lead to a less well-oriented mesogen orientation at the microscopic level compared to our prior findings.

For composite materials, by observing the Debye ring, it can be determined that the composite material exhibits superior orientation compared to the pure material. This may be attributed to the LCE matrix occupying a smaller volume within the composite material. Consequently, a greater deformation is required under the same bending amplitude. Furthermore, it can be observed from the d-space that LCEC has one additional peak compared to LCE and polydomain LCEC. We postulate that this peak provides evidence of a better molecular arrangement of carbon fibers at the microscopic level during the bending and shaping process, leading to the formation of LCEC with improved orientation.

3.2. Thermo mechanical properties

At −50 °C, the material exhibits a high modulus ranging from 2 to 3 GPa. Among all samples, the LCEC demonstrates the highest modulus at

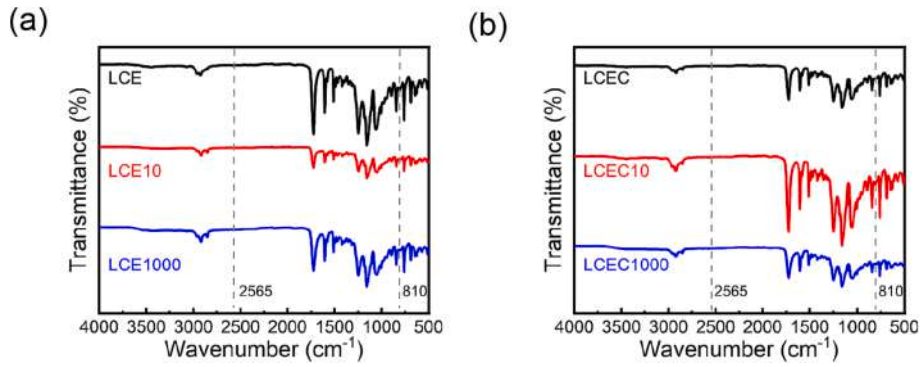

Fig. 2. FTIR of LCE and LCEC synthesized by thiol-acrylate reaction.

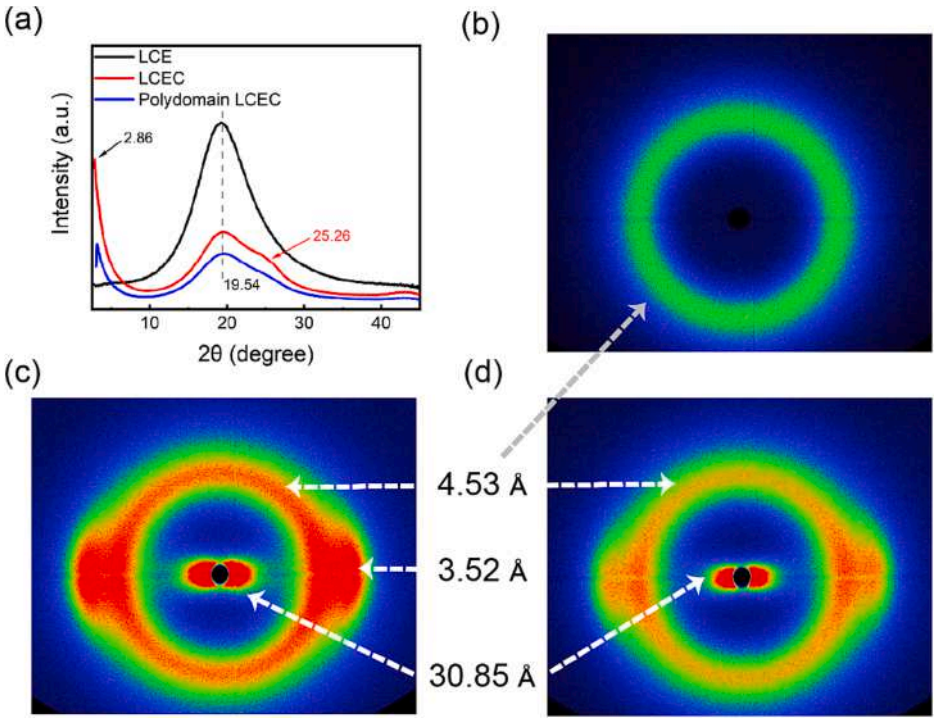

Fig. 3. 2D-WAXD characterizations of LCE samples (a) WARD curves of different samples. The peaks around $2\theta = 2.86$, $2\theta = 19.54$ a and $2\theta = 25.26°$ According to the equation $\lambda = 2d \sin\theta$ ($\lambda = 1.54$ Å), the d-spacing of are 30.85 Å, 4.53 Å, and 3.52 Å; (b) Debye ring of LCE under 25 °C; (c) Debye ring of LCEC under 25 °C; (d) Debye ring of polydomain LCEC under 25 °C.

3.1 GPa. As temperature increases, the polymer reaches rubbery state, with the LCE's modulus dropping to 1.3 GPa at room temperature. With the same condition, the LCEC's modulus reducing to 1.1 GPa. As the temperature continues to rise, the modulus further declines, reaching its lowest point near the transition temperature and then displaying an upward trend. The transition temperature occurs around 50 °C, with a material modulus of 10–20 MPa (Fig. 4**a and 4b**). A detailed summary of the tests performed on the materials can be found in Table 1.

The DMA results demonstrated that the LCE composite had a higher modulus than the pure LCE material, indicating improved mechanical properties. The elastic moduli of the samples were determined at various temperatures, with the curves intersecting at room temperature. The increase in modulus due to the incorporation of carbon fiber reinforcement contributed to the enhanced mechanical performance of the composite materials. Furthermore, none of the loss factor (tan Î) curve displayed two distinct peaks, with all curves featuring a single peak position (Fig. 4**c and 4d**), which represents the polymer's glass transition temperature (T_g). Subsequent experiments confirmed that the material possesses shape memory capabilities according to the T_g. In the absence of a secondary pronounced transition peak within the tan Î curve, the minimum of the storage modulus curve was utilized to determine the nematic-isotropic transition temperature (T_{NI})[37,38]. The T_{NI} values for both LCE and LCEC hover around 85 °C. This observation aligns with subsequent findings wherein, upon heating, the LCE and LCEC initially demonstrate shape memory recovery followed by reversible deformation.

Tensile tests have been conducted to determine the yield stress and fracture strain (Fig. 5). In this assessment, the materials demonstrated varying degrees of fracture stress and fracture strain. Notably, LCE10 and LCEC10 displayed higher fracture stress (approximately 25 MPa), while LCE and LCEC exhibited higher fracture strain (above 50 %). For more detailed data, please refer to Table 2. The results showed that the composites exhibited higher yield stress compared to the pure LCE materials, with an increase in fracture stress observed upon gamma irradiation at certain levels. However, excessively high radiation doses resulted in a decrease in fracture stress. The pure LCE materials displayed higher fracture strains than the composites, indicating their ability to withstand larger deformations before failure.

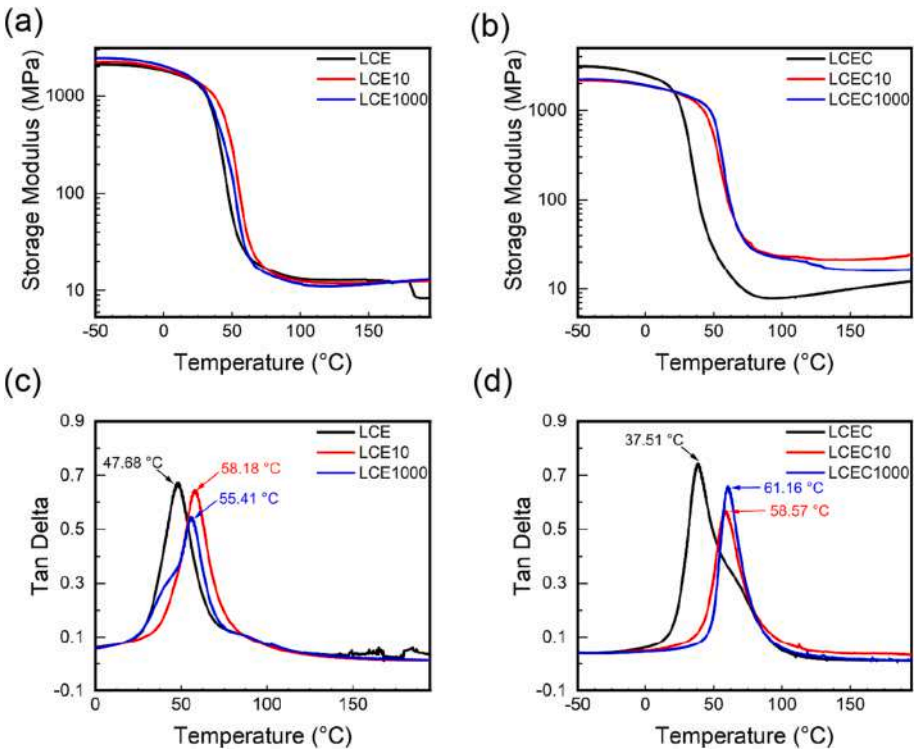

Fig. 4. DMA curves of LCE and LCEC samples with various fiber orientations (a) and (b)The storage modulus of different samples from −50 °C to 200 °C; (c) and (d) The loss factor of different samples from −50 °C to 200 °C.

Table 1
Summary of the mechanical properties of LCE and their composites.

Material	Modulus at −50 °C (MPa)	Modulus at 25 °C (MPa)	T_g. (°C)	Modulus at T_g (MPa)	Max Loss Factor	References
LCE	N/A	About 100	About 22	About 40	About 0.9	[39]
LCE	About 1000	About 1	About 0	About 30	1–2	[38]
LCE	N/A	About 10	32.8–47.8	About 1–3	0.5–0.8	[9]
LCE/eiderdown fiber	N/A	About 110	N/A	N/A	N/A	[24]
LCE	2099.35	1316.73	47.68	90.35	0.66	This work
LCE10	2188.45	1375.87	58.18	60.60	0.64	This work
LCE1000	2419.37	1367.78	55.41	51.19	0.53	This work
LCEC	3104.74	1180.66	37.51	132.49	0.74	This work
LCEC10	2143.77	1532.51	58.57	127.69	0.56	This work
LCEC1000	2204.55	1560.18	61.16	106.84	0.66	This work

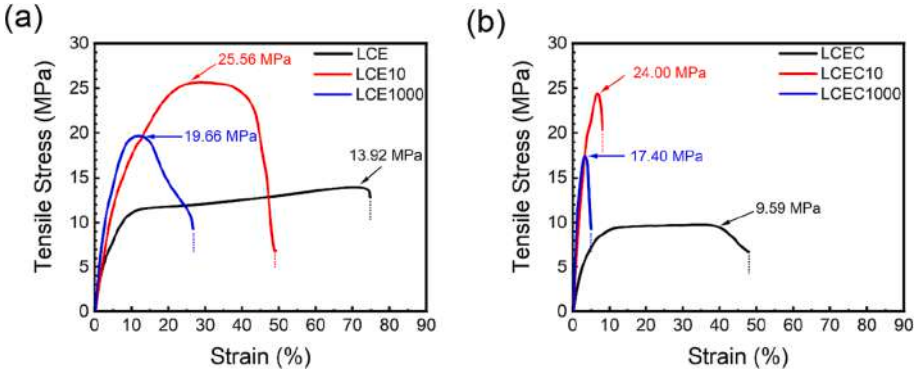

Fig. 5. Tensile test of the LCEs and LCECs under the applied stress at 25 °C.

The DSC and TGA tests were employed to meticulously determine the thermal characteristics of LCE and LCEC. The DSC results indicated that the transformation temperatures of LCE, LCE10, and LCE1000 were observed to be around 32.16 °C (Fig. 6**a**), while those of LCEC, LCEC10, and LCEC1000 were around 23 °C–34 °C (Fig. 6**b**). The DSC results highlight the glass transition temperature. In juxtaposition with the data

Table 2
Summary of the tensile properties of LCE and their composites.

Material	Yield strength (MPa)	Breaking strength (MPa)	Breaking strain (%)
LCE	13.92	12.84	74.78
LCE10	25.56	6.88	49.12
LCE1000	19.66	9.28	26.67
LCEC	9.59	6.74	47.89
LCEC10	24.00	20.36	8.07
LCEC1000	17.40	9.28	4.99

procured via DMA, it is postulated that the transition temperature delineated by DSC represents the commencement of the glass transition. Notably, there is a pronounced alteration in the transition temperature of the LCE composite. Such a deviation is theorized to arise from specialized interactions between the carbon fiber and the LCE matrix, suggesting that the incorporation of carbon fiber can influence the composite material's thermal absorption characteristics. Moreover, the T_{NI} transition peak manifested in the DSC analysis is notably subtle. This observation might be attributed to the minimal overall strain experienced by the sample during its transition from a polydomain to monodomain state. On a microscopic scale, the rotation of the liquid crystal monomer appears to be minimal, which potentially renders the detection of the T_{NI} in DSC challenging. In the TGA test, the onset decomposition temperature of the LCE sample was registered at 337.11 °C, with a maximum decomposition rate temperature of 378.26 °C (Fig. 6**c**). In comparison, the decomposition initiation temperature for the LCEC sample was 320.04 °C, while the peak temperature of decomposition rate recorded was 374.12 °C (Fig. 6**d**). Hence, the carbon fiber didn't significantly affect the thermal stability in samples.

3.3. Reversible deformation and SMP properties

Utilizing traditional methods to transition LCE from a polydomain to a monodomain state often involves stretching the LCE up to 200 %[39]. However, the modulus of our LCE is exceptionally high, and its fracture strain significantly falls short of this benchmark. With a foresight towards subsequent composite experiments, it is imperative to maintain the integrity of the carbon fiber cloth. Hence, extending the sample to 200 % for monodomain fixation is impractical. Consequently, we introduced an innovative method, wherein we shaped the LCE and LCEC into a U-configuration through bending, facilitating the transition from polydomain to monodomain. The subsequent positive outcomes from the reversible transformation and shape memory experiments validate the efficacy of this approach.

First, a reversible deformation test was conducted on the samples. During sample preparation, the samples were bent to 150°, heated to 144.52 °C with a heat gun for 90 s, and subsequently cooled for 300 s. The results demonstrated that the maximum bending angle for LCE was 113.96°, while LCEC achieved 64.98° (Fig. 7, **Movie S1 and S2**). Both materials were able to return to their original angles after cooling. Notably, the bending range of LCEC was significantly larger than that of LCE. We hypothesize that there are two contributing factors to this phenomenon. One reason could be the uneven distribution of carbon fiber layers, which affects the deformation ability of LCEC. The carbon fibre enhances the mechanical properties of the material, which contribute to better recovery performance, as the carbon fibers help maintain the desired shape during cooling and provide additional support for shape recovery upon reheating. Another reason could be that the mesogen within LCEC exhibit a superior orientation. The incorporation of carbon fibers within the LCEC material may lead to better orientation of the mesogen in the LCE. A more organized arrangement of mesogen can enhance the material's ability to fix and recover its shape.

We further conducted shape memory tests on the samples. The samples were compressed to 0° under the action of an external force at 120 °C, cooled to room temperature, and maintained for 5 min before external load has been removed. Subsequently, these samples were reheated under 66.92 °C, at which point they exhibited shape memory deformation. We measured the R_f and R_r of the samples. The results indicated that for LCEC, the R_f was 90 % and the R_r was 99 %, while for

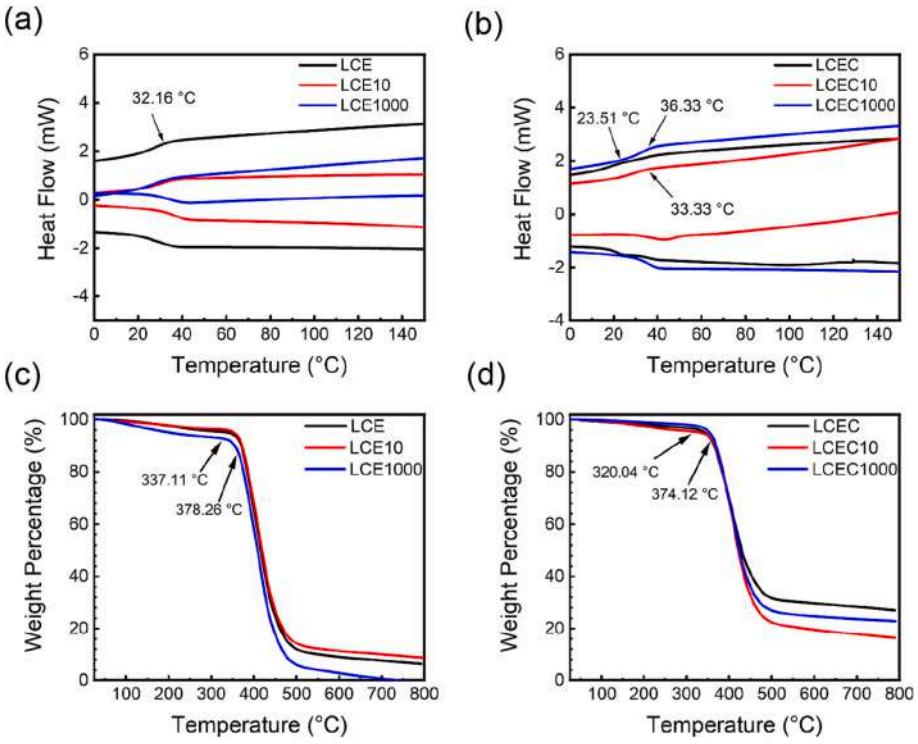

Fig. 6. (a) DSC curves of LCE specimens in N_2 environment; (b) DSC curves of LCEC specimens in N_2 environment; (c) TGA curves of LCE specimens in N_2 environment. (d) TGA curves of LCEC specimens in N_2 environment.

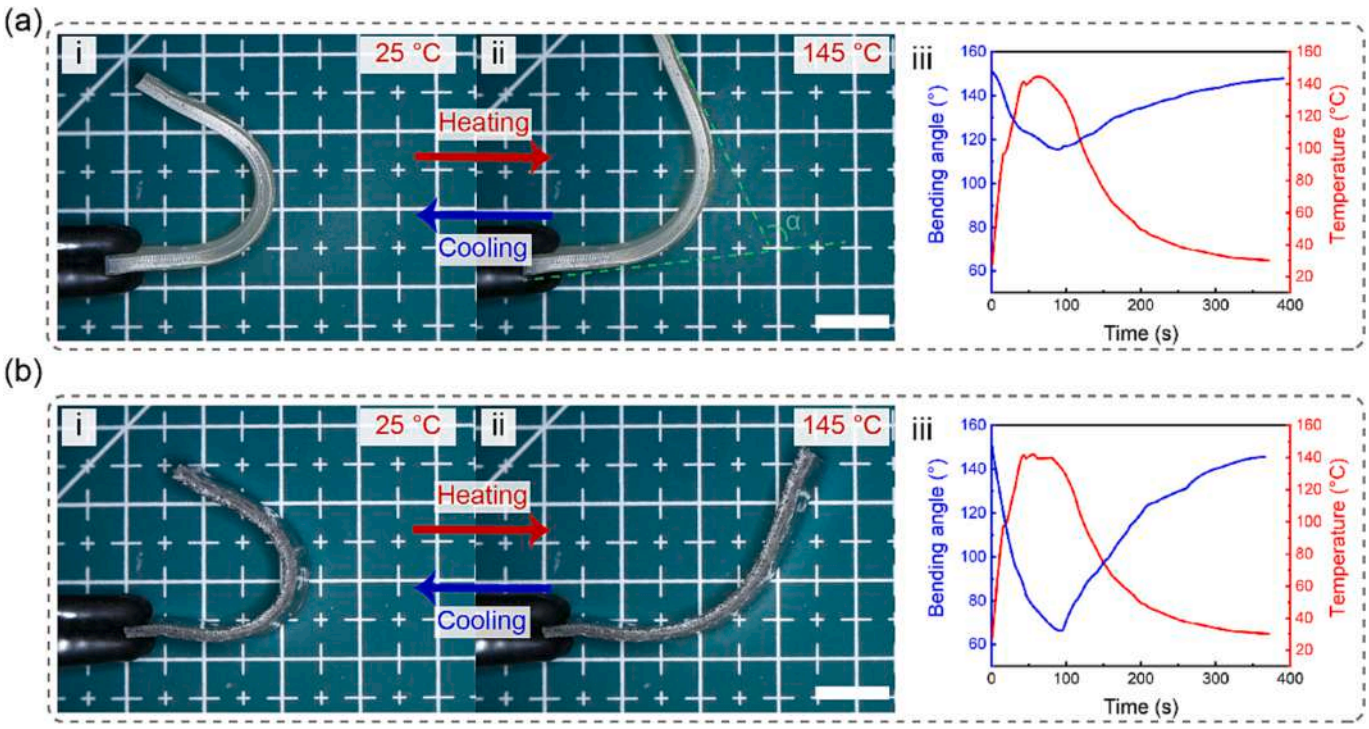

Fig. 7. Reversible thermo transformation behavior of the (a) LCE and (b) LCEC actuator under from room temperature to 144.52 °C. Scale bar: 1 cm.

LCE, the R_f was 85 % and the R_r was 99 %. Both the R_r and R_f of the LCEC composite material are better than those of the pure LCE material (Fig. 8). The evaluated and compared bending angles and corresponding temperatures related to the LCE materials has been demonstrated in **Figure S2 and S3**. We postulate that the enhanced shape memory performance of the LCEC composite arises from the robust interfacial bonding between the LCE matrix and carbon fibers. The presence of this strong interfacial bonding within the composite material can significantly improve the material's shape memory characteristics. The enhanced interface bolsters the overall integrity of the composite, enabling it to preserve its shape more effectively during the cooling process and recover its original shape more efficiently upon reheating. Furthermore, we have accomplished the simultaneous integration of the shape memory effect and reversible deformation effect within a single heating cycle (**Movie S3 and S4**). Subsequent heating of the sample post the shape memory recovery process demonstrated a similar reversible deformation pattern as depicted in Fig. 7. This observed phenomenon underscores a well-defined degree of separation between the T_g and the T_{NI}.

We also carried out shape memory tests and reversible deformation

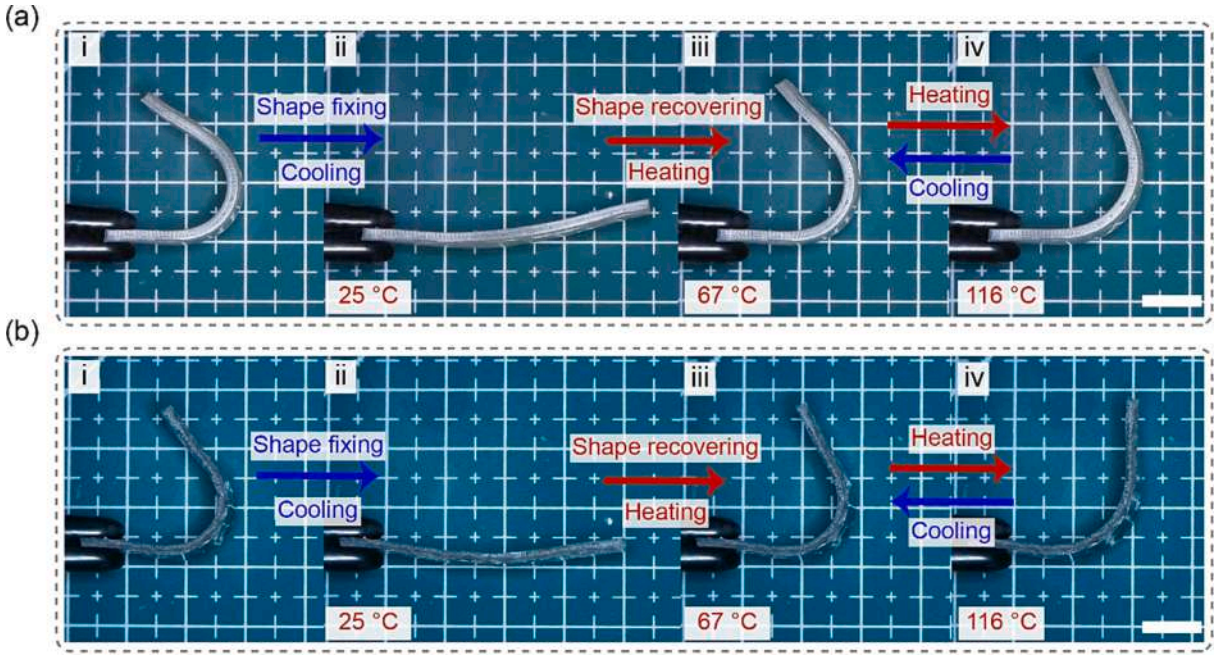

Fig. 8. Shape memory behavior and reversible transformation behavior of the (a)LCE and (b) LCEC actuators. The shape memory behavior was characterized from room temperature to 66.92 °C, while the reversible transformation behavior was characterized from room temperature to 116.45 °C. Scale bar: 1 cm.

tests on samples exposed to gamma-ray irradiation. These results demonstrate reversible transformation ability and shape memory deformation ability of the samples do not exhibit significant changes. The obtained results indicate that gamma-ray irradiation may induce a certain degree of cross-linking and chain scission in the LCE and LCEC materials, potentially affecting their mechanical properties. Nevertheless, these effects do not appear to be substantial enough to significantly impact the samples' reversible deformation and shape memory deformation abilities. Moreover, the inherent structure of the LCE and LCEC materials, encompassing their mesogen orientations and interfacial bonding, remains relatively stable under gamma-ray irradiation. This stability allows the materials to retain their performance characteristics, such as their reversible deformation and shape memory deformation capacities, despite exposure to radiation. Upon consolidating the historical data regarding radiation doses of various materials in outer space (e.g. 408 ± 16Ï¼ Gy/d[40,41]), our findings indicate that LCE and their composite materials possess the capability to function effectively in low Earth orbit for extended periods of time.

3.4. Microstructure

SEM analysis has been conducted to study the microstructure of the LCEC. From the electron microscope results, it can be observed that the matrix in LCE exhibits a uniform texture (Fig. 9**a**). Furthermore, the carbon fibers within LCEC are neatly arranged, and the absence of significant voids in the interfaces the carbon fibre and the LCE substantiates the existence of a robust interfacial bonding between the two components. Fig. 9**b and 9c** display the carbon fiber and matrix distribution at the fracture site of LCEC and LCEC1000, post-tensile testing, respectively. Fig. 9**d** portrays the conjunction of the carbon fiber and matrix of the LCEC after 50 reversible deformations. It is evident that under various conditions, the carbon fiber and LCE matrix exhibit commendable adhesion, and no extensive cracks are discernible. We ascribe this phenomenon to the effective hydrogen bonding established between the carbon fiber and the LCE matrix. This bond safeguards the material's interfacial stability under varying conditions. Furthermore, cross-sectional SEM reveals the positioning of the carbon fiber at the sample's median, as illustrated in **Figure S5**.

Continuing from the electron microscope observations, it is essential to consider how the uniform texture of the LCE matrix and the neatly arranged carbon fibers in LCEC contribute to the overall performance and properties of the materials. The well-organized carbon fiber arrangement in LCEC could potentially enhance the composite's mechanical properties. It is hypothesized that the marked boundary delineating the carbon fiber layer from the material matrix could potentially exert a significant influence on the mechanisms of stress transference and dispersion, thereby improving the composite's overall performance.

4. Conclusions

In our current research, we have embarked on a comprehensive investigation into the mechanical attributes and transformation characteristics inherent to both LCE and its carbon fiber composite counterpart reinforced with unidirectional carbon fiber cloth. From a microscopic perspective, the ester groups present in the LCE matrix are capable of forming hydrogen bonds with the hydroxyl and carboxyl groups residing on the carbon fiber surface. Remarkably, we have successfully attained a breakthrough in enhancing the mechanical properties of LCE, while simultaneously preserving its capacity for reversible deformation and shape memory deformation. Employing two distinct preparation methods, we characterized the samples using a variety of techniques inclusive of spectroscopic analysis, thermodynamic analysis, and microstructure analysis. The outcomes revealed that LCE and LCEC materials exhibited commendable reversible deformation abilities and shape memory performance due to the well-defined T_g and T_{NI}, with LCEC showcasing superior performance in contrast to pure LCE. The gamma-ray irradiation experiments disclosed that both materials retained their reversible deformation and shape memory properties even subsequent to a 1000 KGy exposure, demonstrating their inherent

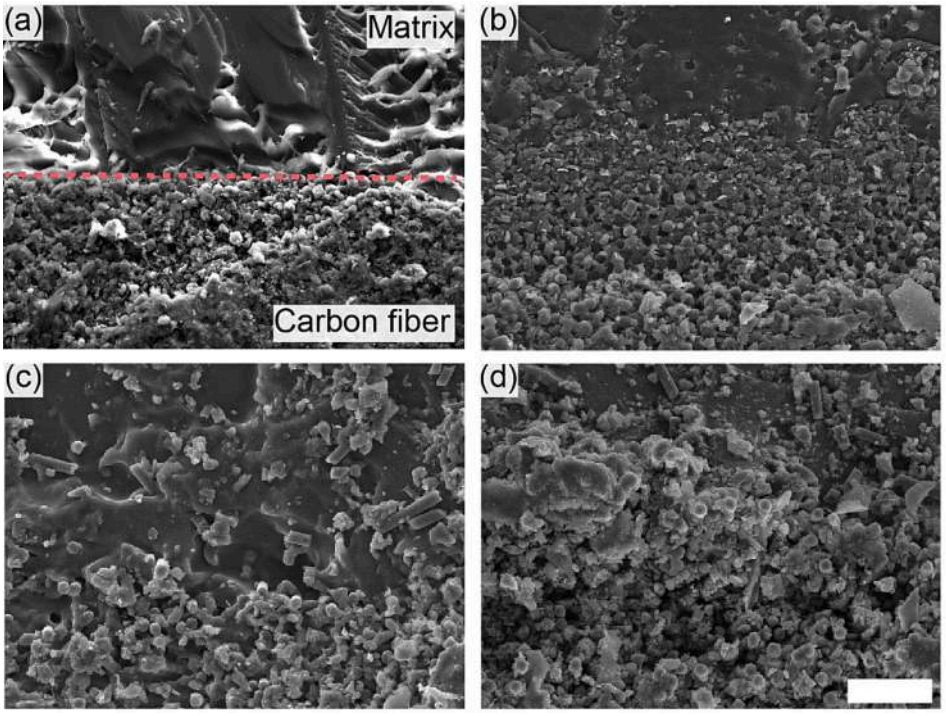

Fig. 9. The SEM images of LCEC samples provided at varying degrees of magnification. (a) The illustration of the distribution of carbon fibers and matrix within the LCEC. (b) Image depicting post-tensile test examination of LCEC. (c) Image depicting post-tensile test examination of LCEC1000. (d) The illustration of LCEC after 50 cycles reversible transformation. Scale bar: 50 Ï¼m.

stability under such circumstances.

In summation, this research offers significant insights into the behavior of LCE and LCEC materials, underscoring their potential for incorporation in smart materials and devices. The comprehensive investigation of LCE and LCEC materials in this study accentuates their prospective application in diverse fields, including aerospace, robotics, and biomedical engineering. Their unique amalgamation of mechanical properties, reversible transformability, shape memory performance, and radiation resistance renders them as promising candidates for further research and development. Presently, LCEC's applicability in aerospace remains limited. It is our aspiration that LCEC, endowed with reversible deformation capabilities, might supersede traditional structures with analogous features—examples being shape memory alloy antennas, variable configurations, actuators, and so on. When juxtaposed with conventional configurations, the LCEC boasts a reduced weight, a characteristic of paramount importance in aerospace endeavors, optimizing the number of components an aerospace apparatus can accommodate. Nonetheless, when contrasted with traditional shape memory alloys, LCEC does exhibit certain limitations, including a diminished actuation force and susceptibility to UV degradation. Future research endeavors aim to address these areas of improvement.

5. Author statement

Initial research directions were identified by Y.X., T.M., and Y.H. Experimental investigations was conducted by Y.X. The paper writing and the figure design were conducted by Y.X. and T.M. All authors contributed to the writing of the manuscript.

Declaration of Competing Interest

The authors declare that they have no known competing financial interests or personal relationships that could have appeared to influence the work reported in this paper.

Data availability

Data will be made available on request.

Acknowledgements

This work is supported by the National Key R&D Program of China (2022YFB3805700).

Appendix A. Supplementary data

Supplementary data to this article can be found online at https://doi.org/10.1016/j.compositesa.2023.107943.

References

[1] Wang Y, Liu J, Yang S. Multi-functional liquid crystal elastomer composites. Appl Phys Rev 2022;9(1):011301.
[2] Fallah-Darrehchi M, Zahedi P, Harirchi P, Abdouss M. Performance of Liquid Crystalline Elastomers on Biological Cell Response: A Review. ACS Appl Polym Mater 2023;5(2):1076–91.
[3] Mu T, Liu L, Lan X, Liu Y, Leng J. Shape memory polymers for composites. Compos Sci Technol 2018;160:169–98.
[4] Xia Y, He Y, Zhang F, Liu Y, Leng J. A Review of Shape Memory Polymers and Composites: Mechanisms, Materials, and Applications. Adv Mater 2021;33(6):2000713.
[5] He Q, Wang Z, Wang Y, Minori A, Tolley MT, Cai S. Electrically controlled liquid crystal elastomer–based soft tubular actuator with multimodal actuation. Sci Adv 2019;5(10).
[6] Bashir M, Rajendran P. A review on electroactive polymers development for aerospace applications. J Intell Mater Syst Struct 2018;29(19):3681–95.
[7] Liu X, Ji H, Liu B, Yang Q. All-solid-state carbon-nanotube-fiber-based finger-muscle and robotic gripper. Int J Smart Nano Mater 2022;13(1):64–78.
[8] Timoshenko PE, Lerer A, Rochal SB. Terahertz frequency selective surfaces using heterostructures based on two-dimensional diffraction grating of single-walled carbon nanotubes. Int J Smart Nano Mater 2023;14(1):21–35.
[9] Burke KA, Mather PT. Soft shape memory in main-chain liquid crystalline elastomers. J Mater Chem 2010;20(17):3449–57.
[10] Guo H, Dai W, Miao Y, Wang Y, Ma D, Xue W. Sustained heparin release actuator achieved from thermal and water activated shape memory hydrogels containing main-chain LC units. Chem Eng J 2018;339:459–67.
[11] Ware Taylor H, McConney Michael E, Wie Jeong J, Tondiglia Vincent P, White TJ. Voxelated liquid crystal elastomers. Science 2015;347(6225):982–4.
[12] Zhai F, Feng Y, Li Z, Xie Y, Ge J, Wang H, et al. 4D-printed untethered self-propelling soft robot with tactile perception: Rolling, racing, and exploring. Matter 2021;4(10):3313–26.
[13] Lv P, Yang X, Bisoyi HK, Zeng H, Zhang X, Chen Y, et al. Stimulus-driven liquid metal and liquid crystal network actuators for programmable soft robotics. Mater Horiz 2021;8(9):2475–84.
[14] Yang X, Chen Y, Zhang X, Xue P, Lv P, Yang Y, et al. Bioinspired light-fueled water-walking soft robots based on liquid crystal network actuators with polymerizable miniaturized gold nanorods. Nano Today 2022;43:101419.
[15] Yang M, Xu Y, Zhang X, Bisoyi HK, Xue P, Yang Y, et al. Bioinspired Phototropic MXene-Reinforced Soft Tubular Actuators for Omnidirectional Light-Tracking and Adaptive Photovoltaics. Adv Funct Mater 2022;32(26).
[16] Yang X, Valenzuela C, Zhang X, Chen Y, Yang Y, Wang L, et al. Robust integration of polymerizable perovskite quantum dots with responsive polymers enables 4D-printed self-deployable information display. Matter 2023;6(4):1278–94.
[17] Zhao J, Zhang L, Hu J. Varied Alignment Methods and Versatile Actuations for Liquid Crystal Elastomers: A Review. Advanced Intelligent Systems 2022;4(3):2100065.
[18] Ohm C, Brehmer M, Zentel R. Liquid Crystalline Elastomers as Actuators and Sensors. Adv Mater 2010;22(31):3366–87.
[19] Liu X, Wei R, Hoang PT, Wang X, Liu T, Keller P. Reversible and Rapid Laser Actuation of Liquid Crystalline Elastomer Micropillars with Inclusion of Gold Nanoparticles. Adv Funct Mater 2015;25(20):3022–32.
[20] Kularatne RS, Kim H, Boothby JM, Ware TH. Liquid crystal elastomer actuators: Synthesis, alignment, and applications. J Polym Sci, Part B: Polym Phys 2017;55(5):395–411.
[21] Xiao Y-Y, Jiang Z-C, Tong X, Zhao Y. Biomimetic Locomotion of Electrically Powered "Janus" Soft Robots Using a Liquid Crystal Polymer. Adv Mater 2019;31(36):1903452.
[22] Saed MO, Ambulo CP, Kim H, De R, Raval V, Searles K, et al. Molecularly-Engineered, 4D-Printed Liquid Crystal Elastomer Actuators. Adv Funct Mater 2019;29(3).
[23] Lu H-F, Nie Z-Z, Bisoyi HK, Wang M, Huang S, Chen X-M, et al. An ultrahigh fatigue resistant liquid crystal elastomer-based material enabled by liquid metal. Sci China Mater 2022;65(6):1679–86.
[24] Zhao N, Wang X, Yao L, Yan H, Qin B, Li C, et al. Actuation performance of a liquid crystalline elastomer composite reinforced by eiderdown fibers. Soft Matter 2022;18(6):1264–74.
[25] Yang L, Setyowati K, Li A, Gong S, Chen J. Reversible Infrared Actuation of Carbon Nanotube-Liquid Crystalline Elastomer Nanocomposites. Adv Mater 2008;20(12):2271–5.
[26] Wang Y, Dang A, Zhang Z, Yin R, Gao Y, Feng L, et al. Repeatable and Reprogrammable Shape Morphing from Photoresponsive Gold Nanorod/Liquid Crystal Elastomers. Adv Mater 2020;32(46):2004270.
[27] Yao L, Yan H, He Y, Zhao N, Wang X, Li C, et al. Actuation performances of catkin fibers reinforced thiol-acrylate main-chain liquid crystalline elastomer. Int J Smart Nano Mater 2022;13(4):668–90.
[28] Herbert KM, Fowler HE, McCracken JM, Schlafmann KR, Koch JA, White TJ. Synthesis and alignment of liquid crystalline elastomers. Nat Rev Mater 2022;7(1):23–38.
[29] Yamada M, Kondo M, Mamiya J-I, Yu Y, Kinoshita M, Barrett C, et al. Photomobile Polymer Materials: Towards Light-Driven Plastic Motors. Angew Chem Int Ed 2008;47(27):4986–8.
[30] Li C, Liu Y, Lo C-w, Jiang H. Reversible white-light actuation of carbon nanotube incorporated liquid crystalline elastomer nanocomposites. Soft Matter 2011;7(16):7511–6.
[31] Kim H, Lee JA, Ambulo CP, Lee HB, Kim SH, Naik VV, et al. Intelligently Actuating Liquid Crystal Elastomer-Carbon Nanotube Composites. Adv Funct Mater 2019;29(48).
[32] Ford MJ, Ambulo CP, Kent TA, Markvicka EJ, Pan C, Malen J, et al. A multifunctional shape-morphing elastomer with liquid metal inclusions. Proc Natl Acad Sci 2019;116(43):21438–44.
[33] Wang L, Zhang F, Liu Y, Leng J. γ-rays radiation resistant shape memory cyanate ester resin and its composites with high transition temperature. Smart Mater Struct 2019;28(7):075039.
[34] Xia Y, Mu T, He Y, Liu Y, Leng J. Fiber-reinforced liquid crystalline elastomer composite actuators with multi-stimulus response properties and multi-directional morphing capabilities. Compos B 2023;256:110640.
[35] Zhang M, Cao M-S, Shu J-C, Cao W-Q, Li L, Yuan J. Electromagnetic absorber converting radiation for multifunction. Mater Sci Eng R Rep 2021;145:100627.
[36] Lee J, Drzal LT. Surface characterization and adhesion of carbon fibers to epoxy and polycarbonate. Int J Adhes Adhes 2005;25(5):389–94.
[37] Merkel DR, Traugutt NA, Visvanathan R, Yakacki CM, Frick CP. Thermomechanical properties of monodomain nematic main-chain liquid crystal elastomers. Soft Matter 2018;14(29):6024–36.

[38] Mistry D, Traugutt NA, Sanborn B, Volpe RH, Chatham LS, Zhou R, et al. Soft elasticity optimises dissipation in 3D-printed liquid crystal elastomers. Nat Commun 2021;12(1).
[39] Yu L, Shahsavan H, Rivers G, Zhang C, Si P, Zhao B. Programmable 3D Shape Changes in Liquid Crystal Polymer Networks of Uniaxial Orientation. Adv Funct Mater 2018;28(37):1802809.
[40] Berger T, Hajek M, Bilski P, Körner C, Vanhavere F, Reitz G. Cosmic radiation exposure of biological test systems during the EXPOSE-E mission. Astrobiology 2012;12(5):387–92.
[41] Benton ER, Benton EV. Space radiation dosimetry in low-Earth orbit and beyond. Nucl Instrum Methods Phys Res, Sect B 2001;184(1):255–94.